Energetic electron-bunch generation in a phase-locked longitudinal laser electric field

K. D. Xiao,[1] T. W. Huang,[1] L. B. Ju,[2] R. Li,[1] S. L. Yang,[1] Y. C. Yang,[1] S. Z. Wu,[3] H. Zhang,[3]
B. Qiao,[1,4,5] S. C. Ruan,[6] C. T. Zhou,[1,3,6,*] and X. T. He[1,3]

[1]*Center for Applied Physics and Technology, HEDPS, and School of Physics, Peking University, Beijing 100871, People's Republic of China*
[2]*Graduate School, China Academy of Engineering Physics, P.O. Box 2101, Beijing 100088, People's Republic of China*
[3]*Institute of Applied Physics and Computational Mathematics, Beijing 100094, People's Republic of China*
[4]*State Key Laboratory of Nuclear Physics and Technology, Peking University, Beijing 100871, People's Republic of China*
[5]*Collaborative Innovation Center of Extreme Optics, Shanxi University, Taiyuan, Shanxi, 030006, People's Republic of China*
[6]*College of Electronic Science and Technology, Shenzhen University, Shenzhen 518060, People's Republic of China*

(Received 14 February 2016; revised manuscript received 30 March 2016; published 25 April 2016)

Energetic electron acceleration processes in a plasma hollow tube irradiated by an ultraintense laser pulse are investigated. It is found that the longitudinal component of the laser field is much enhanced when a linear polarized Gaussian laser pulse propagates through the plasma tube. This longitudinal field is of $\pi/2$ phase shift relative to the transverse electric field and has a π phase interval between its upper and lower parts. The electrons in the plasma tube are first pulled out by the transverse electric field and then trapped by the longitudinal electric field. The trapped electrons can further be accelerated to higher energy in the presence of the longitudinal electric field. This acceleration mechanism is clearly illustrated by both particle-in-cell simulations and single particle modelings.

DOI: 10.1103/PhysRevE.93.043207

I. INTRODUCTION

Energetic electron beams generated by ultraintense laser plasma interactions have attracted great attention because of their broad applications, such as fast ignition of inertial confined fusion, radiography, synchrotron radiation, and proton acceleration, etc. [1–10]. Recently, a plasma hollow cylinder tube has been employed to accelerate and collimate energetic electron beams [11–22]. Since the electrons can be guided through the balance between electric field force and $\mathbf{v}\times\mathbf{B}$ force, these generated electrons are therefore collimated by the plasma tube [15,19–21]. Furthermore, it was found that the tube structure can be used to generate high-quality attosecond electron bunches, which provides a quite useful source to generate ultrabright x-ray, γ-ray, and positron beams [11–14,16,18,22]. Although electron guiding and collimation mechanisms have been clear, the electron acceleration mechanism in the plasma tube is not reported yet.

It is known that electrons in plasmas can be accelerated by the ponderomotive force when an intense laser pulse irradiates a plasma foil. These electrons obtain energy from the transverse laser electric field and then the energy is transferred to the longitudinal direction by the Lorentz force [23–25]. The effect of the longitudinal laser electric field of a Gaussian laser pulse on the electron acceleration is usually neglected because its magnitude is much smaller than the transverse electric field [26]. As a contrast, the electron acceleration in the plasma tube is possibly of very different behavior. We recall that the electromagnetic mode switching in nonlinear optics can take place when an electromagnetic wave propagates in a narrow hollow waveguide in which the corresponding longitudinal electric field may be much enhanced [27–29]. Whether this behavior could also be observed in relativistic laser plasma interaction is an interesting question.

In this paper, we investigate the energetic electron acceleration mechanism by irradiating an ultraintense laser pulse into the plasma hollow tube. Our two-dimensional particle-in-cell simulations along with single particle modelings clearly show that the longitudinal component of laser fields is much enhanced with the optical confinement by the tube edge, which is inducted by the increment of the laser transverse electric field gradient. With the formation of the enhanced longitudinal field, it is demonstrated that the electron is not only well guided in the tube but also accelerated adequately to higher energy that is much beyond the ponderomotive scaling law. The paper is arranged as follows. The descriptions of our target configuration and simulation setup are given in Sec. II. The generation of the longitudinal electric field and the acceleration of electron bunches are investigated in Sec. III. The relation between electron energy and target parameters is also discussed. Then Sec. IV gives our main conclusion.

II. SIMULATION SETUP

The target configuration is shown in Fig. 1, where the plasma hollow tube irradiated by an ultraintense laser pulse is shown. The length of the plasma hollow tube is 50 μm. Its inner diameter and wall thickness are $d_0 = 4$ μm and 2 μm, respectively. The tube consists of copper plasmas with a constant degree of ionization $Z = 2$ and the electron number density $n_{e0} = 50n_c$, where $n_c = m_e\epsilon_0\omega_0^2/e^2$ is a critical number density. The intense laser pulse is a linearly y-polarized laser with intensity of 2×10^{20} W/cm^2 ($a_0 = 12.8$) and wavelength of 1.06 μm. The laser period is defined as $T_0 = 2\pi/\omega_0$. The laser pulse has a spatially Gaussian profile $a = a_0\exp(-y^2/\sigma^2)$, with $\sigma = 4$ μm and a temporally flat-top profile with duration of $\tau = 30$ fs. In our two-dimensional particle-in-cell (PIC) simulations, the simulation box is chosen as 60 μm in the longitudinal x direction and 20 μm in the

*zcangtao@iapcm.ac.cn

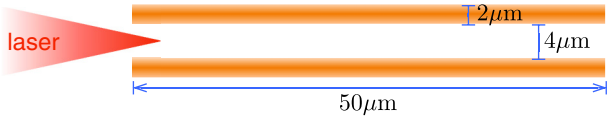

FIG. 1. Target configuration in simulations. A short pulse laser irradiates and injects into a hollow tube.

transverse y direction. The spatial grid is set as 5030×1677, and each cell is filled in 50 ions and 150 electrons [30].

III. LONGITUDINAL ELECTRIC FIELD GENERATION AND ELECTRON ACCELERATION

For an electromagnetic wave in the form of $\mathbf{E}(\mathbf{x},t) = \tilde{\mathbf{E}}(\mathbf{x})e^{i(\mathbf{k}\cdot\mathbf{x}-\omega_0 t)}$, one can get that $\nabla^2\tilde{\mathbf{E}} + k^2\tilde{\mathbf{E}} = 0$ and $\nabla\cdot\tilde{\mathbf{E}} = 0$ from the Maxwell equations. If the wave is supposed to propagate in the positive x direction, in the case of $E_z = 0$, the longitudinal electric field with $\tilde{E}_x = \frac{i}{k}\frac{\partial\tilde{E}_y}{\partial y}$ can be obtained. For a plane wave, it has no E_y gradient and thus the field $E_x = 0$. For a Gaussian laser beam in free space with $E_y = E_0\exp(-y^2/\sigma^2)\cos(kx-\omega_0 t)$, the longitudinal component is in the form of $E_x = \frac{2y}{k\sigma^2}E_0\exp(-y^2/\sigma^2)\sin(kx-\omega_0 t)$, which is small relative to the E_y field. As for laser parameters used in simulations, the amplitude of the longitudinal laser field in vacuum is only about $0.03E_0$.

However, when a Gaussian laser beam is injected into the narrow tube, the laser field distribution would be quite different from that in vacuum. Both laser longitudinal and transverse electric fields inside the tube are illustrated in Fig. 2. It is shown that due to the optical confinement, the intensity of the laser pulses is increased and the spot radius is reduced [see Fig. 2(c)]. Moreover, the spatial profile of the laser field is modulated by the finite distance between the upper and lower tube walls, which results in the formation of a super-Gaussian beam. The corresponding longitudinal component of the focused laser field in the tube is approximately expressed as $E_x \approx \frac{ny^{n-1}}{k\sigma'^n}E_0'\exp(-y^n/\sigma'^n)\sin(kx-\omega_0 t)$, where the range of n is $4\sim 6$, and E_0' and σ' denote the amplitude and spot radius of the focused laser field, respectively [8]. Thus the longitudinal field is much increased in the narrow tube compared with that in vacuum. Figure 2(a) clearly illustrates that the amplitude of the longitudinal laser field is approximately a quarter of the transverse laser field. The E_x field is $\pi/2$ phase shifted relative to the E_y field [see Fig. 2(a)] and has π phase interval between upper and lower parts of the wave [see Fig. 2(b)]. This shifting behavior between the E_y and E_x fields as shown in Figs. 2(b) and 2(c) then results in the electron bunches shifting as shown in Fig. 2(d). Electrons at the upper (lower) edge of the tube are first pulled out by the positive (negative) transverse electric field E_y into the vacuum. These electrons forming electron bunches are separated by a laser wavelength on each side. The lower electron bunches are π phase shifted relative to the upper ones [15,21] [also see Fig. 2(d)]. These electrons are finally accelerated by the combination of both laser longitudinal and transverse electric fields.

To clarify the acceleration process of these electron bunches inside the tube, we use particle tracing methods in our PIC simulations. In order to clearly illustrate the energy gain of

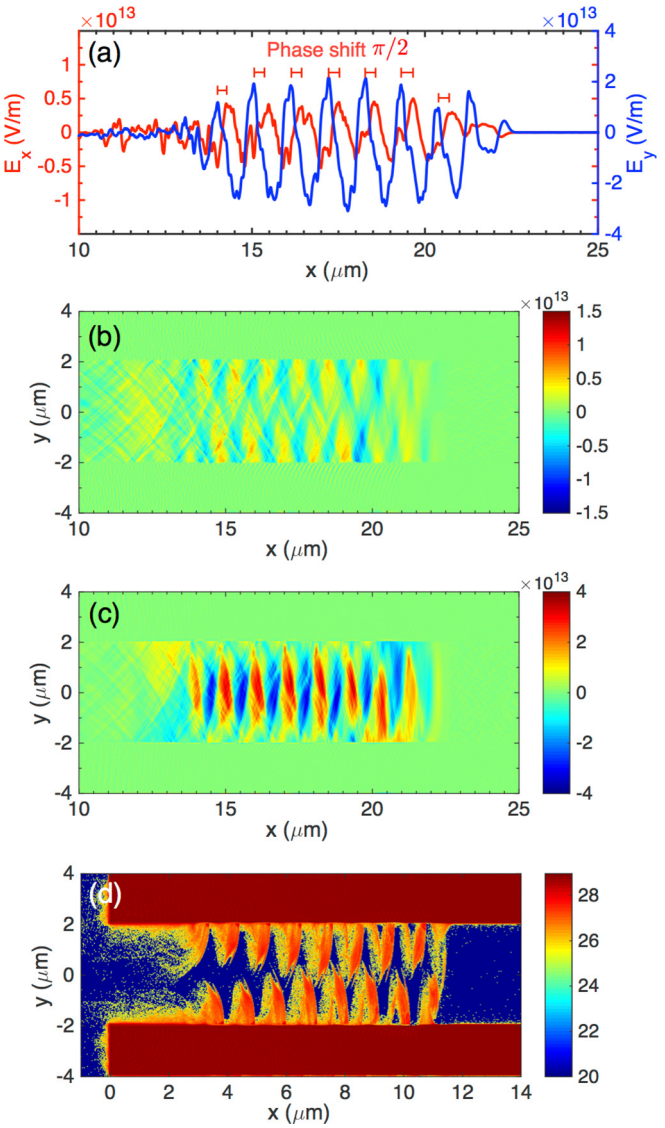

FIG. 2. Both longitudinal (red or light gray) and transverse (blue or dark gray) laser electric fields in the plasma tube. (a) The profile of both fields at the upper tube edge. (b) The longitudinal electric field E_x, and (c) the transverse electric field E_y in units of V/m. (d) The electron number density in log scale with unit of m^{-3}.

the accelerated electron, we furthermore separate the energy of each electron into two parts, i.e.,

$$\epsilon = \epsilon_\parallel + \epsilon_\perp, \tag{1}$$

where $\epsilon_\parallel$ is the energy gain in parallel direction,

$$\epsilon_\parallel = -\int_0^t ev_x E_x dt, \tag{2}$$

and $\epsilon_\perp$ is the energy gain in perpendicular direction,

$$\epsilon_\perp = -\int_0^t e(v_y E_y + v_z E_z)dt. \tag{3}$$

The trajectories of the traced electron energy gain in the $\epsilon_\parallel$ and $\epsilon_\perp$ plane are shown in Fig. 3, which indicates that the energetic electrons are clearly separated into two groups. The electrons obtain most of their energy at the parallel direction (as group

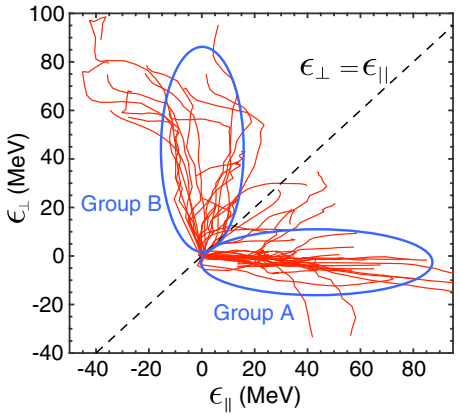

FIG. 3. The trajectories of energy gain in both parallel and perpendicular directions for traced energetic electrons.

A) and at the perpendicular direction (as group B), whereas there are only a few electrons which obtain their energy at two directions simultaneously.

The corresponding spatial trajectories for traced electrons are illustrated in Fig. 4. It is shown that the electron can be accelerated to a high energy of nearly 100 MeV, while we note that only $\epsilon_{\rm pond} \approx m_e c^2 a_0^2/2 = 42$ MeV electron energy can be obtained by the ponderomotive potential in vacuum. When the plasma hollow tube is irradiated by the ultraintense laser pulse, the electrons are first pulled out from the tube edge by the E_y field. These electrons are then trapped and accelerated by the laser field with the pattern of separate electron bunches for a long distance, as shown in Fig. 2(d). For group A, the electrons are mainly accelerated by the longitudinal electric field E_x, while a small fraction of energy gain is obtained from the laser ponderomotive force [see Figs. 4(b) and 4(c)]. From the corresponding electron trajectories shown in Fig. 4(a), we can see that these electrons have little transverse y-direction displacements and are well guided in the longitudinal x direction, which means that the force balance between E_y and $v_x B_z$ is achieved in the y direction. On the other hand, for group B, the electrons are mainly accelerated by the ponderomotive force, while little energy gain is obtained from the longitudinal electric field [see Figs. 4(e) and 4(f)]. From the electron trajectories shown in Fig. 4(d), these electrons are bounced back and forth between the upper and lower tube edges by the E_y field. When these electrons hit the tube edge, they are then reflected by the strong radial static interface electric field, which is generated by the electron bunches. In this case, the electron acceleration process is interrupted and the energy gain of the electron is also retarded [see Figs. 4(d) and 4(e)]. After this reflection, the electrons can then be trapped by the laser field again and continue the acceleration processes.

The dominated electron acceleration process is determined by the hot electron numbers in each energy gain source. We counted up electron numbers for $\epsilon_\parallel > \epsilon_\perp$ and $\epsilon_\parallel < \epsilon_\perp$, respectively, at every time, as shown in Fig. 5(a). The hot electron number is increased in early $25T_0$ and then reaches its saturation. It is found that the longitudinal acceleration devotes about 65% of the final hot electrons, and the ponderomotive acceleration devotes about 35%. This indicates that the longitudinal laser electric field plays a dominant role in the

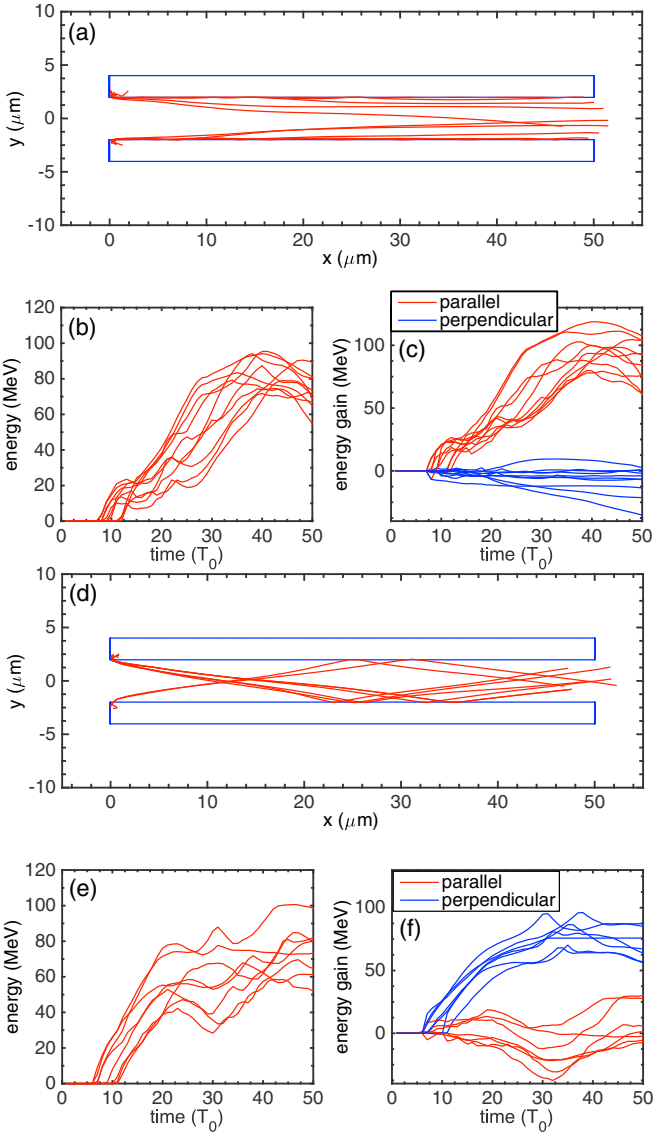

FIG. 4. Acceleration processes for traced electrons. These electrons are divided into two groups (see context for details). Group A (a)–(c) for electrons which mainly obtain energy in the parallel direction, where the longitudinal electric field dominates. Group B (d)–(f) for electrons which mainly obtain energy in the perpendicular direction, where the ponderomotive force dominates. Subplots (a) and (d) for electron trajectories, (b) and (e) for total energy, (c) and (f) for energy gain source, respectively.

high-energy electron acceleration. The evolution of maximum electron energy is shown in Fig. 5(b) and the electron energy spectrum is shown in Fig. 5(c). It is exhibited that the electrons in the tube form a broad peak spectrum with peak energy of 55 MeV and a maximum energy of 120 MeV, which is much higher than the value in vacuum by interacting with the same laser pulse. The broad peak spectrum is the result of electron injection. As it is shown by Figs. 4(a) and 4(d), the electron injection mainly occurs at the entrance of the plasma tube when each cycle of the laser pulse starts entering into the tube. Once the laser pulse is completely entered in, the electrons at the tube edge are prevented from injection because of the strong

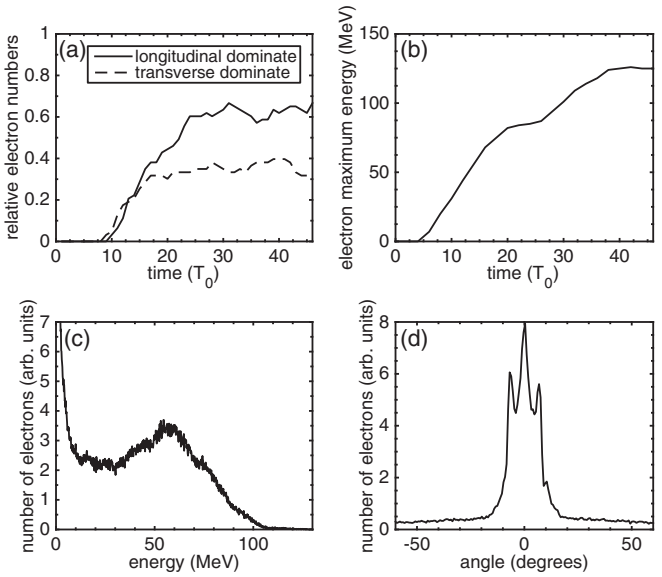

FIG. 5. (a) Statistic of energetic electron (with energy greater than 20 MeV) numbers for electrons mainly obtained energy from the longitudinal electric field ($\epsilon_\parallel > \epsilon_\perp$) or the transverse electric field ($\epsilon_\parallel < \epsilon_\perp$), normalized by the final total energetic electron numbers. (b) Electron maximum energy varying with time. (c) Electron energy spectrum and (d) electron divergence angle for electrons in the tube at time $t = 42\mathrm{T}_0$ when the acceleration is saturated.

radial static electric field generated by electron bunches, and thus the injection process is terminated. Due to this injection, the energetic electrons are accelerated as a whole, starting from the tube entrance. Therefore, the broad peak spectrum is generated. Through our estimation, the total electron number exiting the tube is approximately 6×10^{10} ($\sim nC$). The electron divergence angle is about 10° at the final time featured with three peaks, as shown in Fig. 5(d), which is lower than that in the normal cases [31]. According to the analysis given in Fig. 4, the electrons undergoing longitudinal acceleration are well guided and have a rather low divergence angle, which corresponds to the central peak. The electrons undergoing ponderomotive acceleration bounce between tube edges and have a larger divergence angle, which contributes to two small peaks at each side of the central peak. This collimated energetic electron beam can be applied as an important intermediate for proton acceleration [11,22], bright x-ray [13,14,16], γ-ray and positron [12,18] beam generation, etc. For example, in proton acceleration, by attaching a foil at the end point of the tube, this well-guided electron beam generates a localized and enhanced sheath field at the target rear surface. As a result, the protons can be accelerated by this field to a much higher energy relative to the normal bare foil target [11,22].

For further illustration of the electron acceleration mechanism, a simplified single particle model which is abstracted from previous PIC simulation results is also considered. A free electron initially at rest is supposed to move in a combined field, which is composed of a laser field E_y (B_z), where $|E_y| = c|B_z|$, and a small-amplitude longitudinal periodic electric field E_x. The equations of motion for the considered

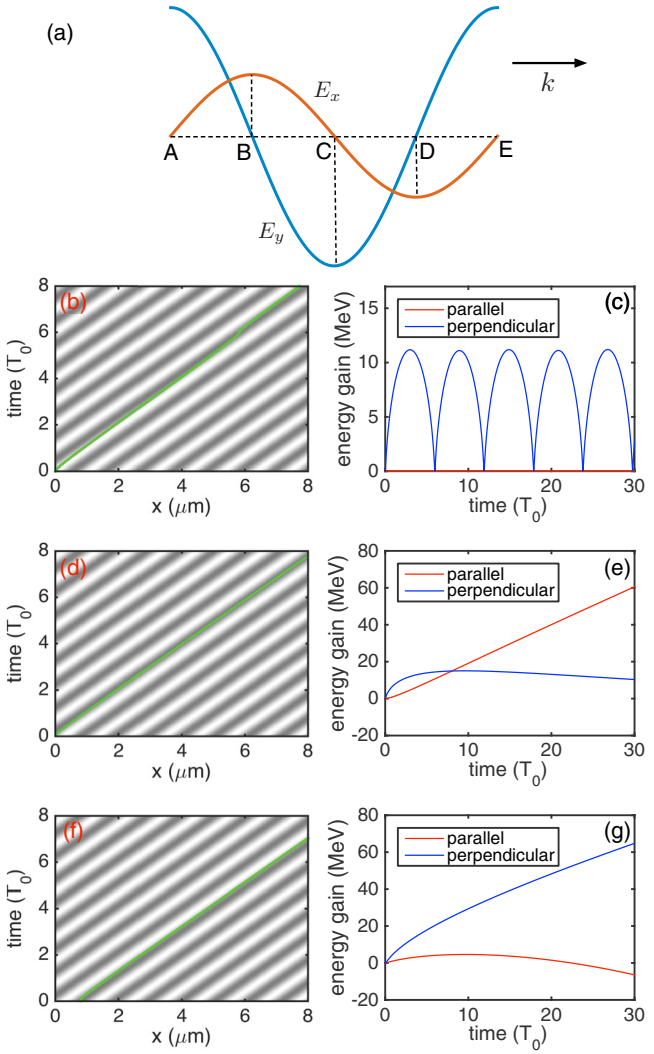

FIG. 6. Numerical results for single particle model, where a combined planar laser field of $E_y = 2 \times 10^{13}$ V/m and $\pi/2$ phase shifted $|E_x| = 0.1|E_y|$ is supposed. (a) The laser electric fields and definitions of points. (b, c) Electron motion in $E_x = 0$ case as a contrast. (d, e) Electron motion with initial phase at point A (E). (f, g) Electron motion with initial phase at point D. The relations between fields and electron trajectories are shown in (b), (d), and (f). The field shown in (b) is E_y, in (d) and (f) are E_x. Panels (c), (e), and (g) show the electron energy gain.

electron are

$$\frac{dp_x}{dt} = -eE_x - ev_yB_z, \tag{4}$$

$$\frac{dp_y}{dt} = -eE_y + ev_xB_z, \tag{5}$$

$$\frac{d\gamma}{dt} = -\frac{ev_xE_x}{m_ec^2} - \frac{ev_yE_y}{m_ec^2}, \tag{6}$$

where $\gamma = \sqrt{1 + (p_x^2 + p_y^2)/(m_e^2c^2)}$ is relativistic factor.

It is supposed that electrons have different initial positions with different phases. The definitions of point positions and phase relations are shown in Fig. 6(a), where the E_x field is $\pi/2$ phase shifted relative to the E_y field [the same as Fig. 2(a)]. The point A (E) is the maximum point of the E_y field and zero point

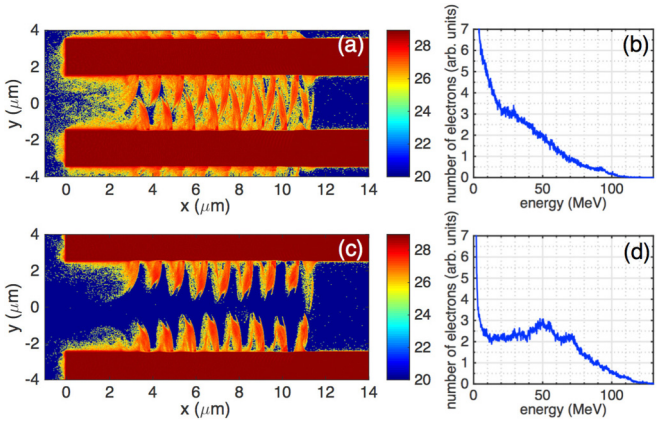

FIG. 7. Electron number density in log scale with unit of m^{-3}, and energy spectrum for electrons in the tube at time $t = 42T_0$. (a, b) Tube with inner diameter of $d_0 = 3$ μm and (c, d) tube with inner diameter of $d_0 = 5$ μm.

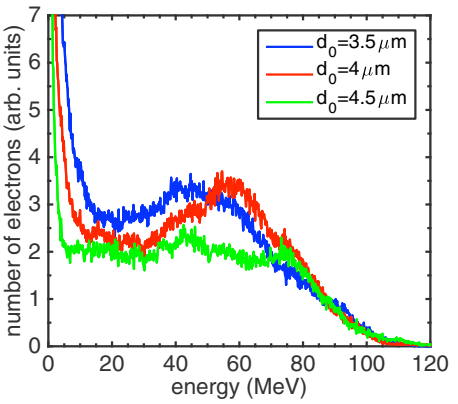

FIG. 8. Comparison of electron energy spectrums for tubes with diameters near $d_0 = 4$ μm at time $t = 42T_0$.

of the E_x field. The electron at this point is initially at the edge of the negative acceleration E_x field valley accompanied with the E_y field crest. It is most likely to be trapped by the E_x field and obtains most of its energy at the longitudinal direction [see Figs. 6(d) and 4(e)]. Compared with the high-frequency quiver trajectories in the E_x absence case [see Figs. 6(b) and 6(c)], the electron in the E_x existence case comoves with the E_x field. Thus, the acceleration length is much increased. As a result, the electron energy can reach a value much higher than laser ponderomotive potential. Point D is the zero point of the E_y field and the maximum point of the E_x field. The electron at this point is initially at the beginning of the ponderomotive force acceleration phase accompanied by a negative acceleration E_x field background. It is most likely to be accelerated by ponderomotive force in the transverse direction [see Figs. 6(f) and 6(g)]. From Eqs. (4)–(6), the electron dephasing rate can be defined as [25]

$$R = \gamma - \frac{p_x}{m_e c} = 1 + \frac{e}{m_e c}\int E_x d\tau, \tag{7}$$

where $\tau = t - x/c$. It is known that $R = 1$ is for the E_x absence case, i.e., normal case which contains only E_y and B_z fields. For an electron initially at point D, its dephasing rate R is reduced by the negative E_x field to be $R < 1$. Thus, the electron can be accelerated for a longer distance before entering into the dephasing point.

The acceleration of electrons initially at B and C points are noneffective at this situation. The E_x field at these points is in a positive direction, which results in the corresponding dephasing rate $R > 1$. The electron acceleration length is thus reduced. Because of the π phase shift between the upper and lower parts of the focused E_x field in the tube [see Fig. 2(b)], these electrons can be effectively accelerated by another part of the field, where negative acceleration of the E_x field dominates. In such a way, the generation of energetic electron bunches, which are separated by a laser wavelength on one side and π phase shifted between two sides of the tube, has been fully explained [see Fig. 2(d)].

The dependence of electron properties on different tube diameters is also studied. The simulation results are shown in Fig. 7. For a thinner tube with $d_0 = 3$ μm, when the laser is injecting into the hollow tube, an underdense plasma is generated inside the tube due to electron diffusion in this narrow channel [see Figs. 7(a) and 7(b)]. This underdense plasma is an obstacle to the propagation of the laser field and the longitudinal electric field. The electron acceleration is thus less effective and there is no generation of electron bunches of the broad peak spectrum [see Figs. 5(c) and 7(b)]. However, for a wider tube with $d_0 = 5$ μm, see Figs. 7(c) and 7(d), the focusing of the laser field during laser injection into the tube is less effective than the $d_0 = 4$ μm case and the longitudinal electric field is rather weaker. Furthermore, the electron bunches are mostly accelerated by the edge part of the laser spot rather than the central part in the $d_0 = 4$ μm case. That means the quality of electron bunches accelerated by a wider tube is lowered [see Figs. 5(c) and 7(d)]. For tubes with diameters near the optimum choice of $d_0 = 4$ μm, the corresponding electron energy spectrum has a better peak structure (see Fig. 8). It is therefore suggested that a suitable tube can be used to accelerate electrons to achieve a higher quality. In addition, considering the injection process of high-energy electrons, it is inferred that the electron energy spectrum can be further optimized by using a few-cycle laser pulse.

IV. CONCLUSION

In summary, we investigate energetic electron acceleration processes by irradiating an ultraintense laser pulse into a plasma hollow tube. Using two-dimensional particle-in-cell simulations as well as analyzing single particle trajectories, we find that the electron acceleration mechanism in the plasma hollow tube is quite different from the bare foil case where the ponderomotive force dominates. As far as the plasma tube is concerned, the longitudinal laser electric field of a Gaussian laser beam becomes important to accelerate the electron due to the optical confinement by the tube edge. The majority of energetic electrons is accelerated by the longitudinal field, while only a small fraction of the electrons obtain their energy from the transverse laser field. This acceleration mechanism is clearly verified by our single particle modeling. Furthermore, we show that the acceleration

process of an electron obviously depends on its injection phase relative to the laser field. Because of their π phase shift of the upper and lower longitudinal electric field components, the electrons accelerated inside the plasma tube exhibit a π phase shift and form the so-called separated electron bunches. Through use of the plasma tube, the accelerated electron bunches are of high quality with a broad peak spectrum and a low divergence angle, which has broad applications in high-energy-density plasmas, such as in proton acceleration, neutron production, fast ignition in inertial confinement fusion, bright radiation source generation, and position production, etc.

ACKNOWLEDGMENTS

This work is supported by the National Natural Science Foundation of China (Grants No. 91230205, No. 11575031, No. 11575298, and No. 11175026), the National Basic Research 973 Project, No. 2013CB834100, and the National High-Tech 863 Project. The computational resources are supported by the Special Program for Applied Research on Super Computation of the NSFC-Guangdong Joint Fund (the second phase). B.Q. acknowledges support from the Thousand Young Talents Program of China. K.D.X. would like to thank K. Q. Pan, Y. X. Zhang, and C. Z. Xiao for fruitful discussions.

[1] M. Tabak, J. Hammer, M. E. Glinsky, W. L. Kruer, S. C. Wilks, J. Woodworth. E. M. Campbell, and M. D. Perry, Phys. Plasmas **1**, 1626 (2004).
[2] P. A. Norreys, R. Allott, R. J. Clarke, J. Collier, D. Neely, S. J. Rose, M. Zepf, M. Santala, A. R. Bell, K. Krushelnick, A. E. Dangor, N. C. Woolsey, R. G. Evans, H. Habara, T. Norimatsu, and R. Kodama, Phys. Plasmas **7**, 3721 (2000).
[3] X. T. He, H. Cai, S. Wu, L. Cao, H. Zhang, M. He, M. Chen, J. Wu, C. Zhou, W. Zhou, L. Shan, W. Wang, F. Zhang, B. Bi, Z. Zhao, Y. Gu, B. Zhang, W. Wang, Z. Fang, A. Lei, C. Wang, W. Pei, and S. Fu, Plasma Phys. Control. Fusion **57**, 064003 (2015).
[4] C. T. Zhou and X. T. He, Appl. Phys. Lett. **90**, 031503 (1997); C. T. Zhou, X. T. He, and L. Y. Chew, Opt. Lett. **36**, 924 (2011).
[5] E. Esarey, C. B. Schroeder, and W. P. Leemans, Rev. Mod. Phys. **81**, 1229 (2009).
[6] S. Corde, K. T. Phuoc, G. Lambert, R. Fitour, V. Malka, and A. Rousse, Rev. Mod. Phys. **85**, 1 (2013).
[7] W. P. Leemans, A. J. Gonsalves, H.-S. Mao, K. Nakamura, C. Benedetti, C. B. Schroeder, Cs. Toth, J. Daniels, D. E. Mittelberger, S. S. Bulanov, J.-L. Vay, C. G. R. Geddes, and E. Esarey, Phys. Rev. Lett. **113**, 245002 (2014).
[8] A. Pukhov, Rep. Prog. Phys. **65**, R1-R55 (2002).
[9] A. Macchi, M. Borghesi, and M. Passoni, Rev. Mod. Phys. **85**, 751 (2013).
[10] K. D. Xiao, C. T. Zhou, B. Qiao, and X. T. He, Phys. Plasmas **22**, 093112 (2015); K. D. Xiao, T. W. Huang, C. T. Zhou, B. Qiao, S. Z. Wu, S. C. Ruan, and X. T. He, AIP Adv. **6**, 015303 (2016).
[11] K. H. Pae, I. W. Choi, S. J. Hahn, J. R. Cary, and J. Lee, Phys. Plasmas **16**, 073106 (2009).
[12] X. L. Zhu, Y. Yin, T. P. Yu, F. Q. Shao, Z. Y. Ge, W. Q. Wang, and J. J. Liu, New J. Phys. **17**, 053039 (2015).
[13] Z. Lecz and A. Andreev, Phys. Rev. E **93**, 013207 (2016).
[14] L. Yi, A. Pukhov, P. Luu-Thanh, and B. Shen, Phys. Rev. Lett. **116**, 115001 (2016).
[15] S. Jiang, A. G. Krygier, D. W. Schumacher, K. U. Akli, and R. R. Freeman, Phys. Rev. E **89**, 013106 (2014).
[16] K. V. Lotov, K. V. Gubin, V. E. Leshchenko, V. I. Trunov, and E. V. Pestryakov, Phys. Plasmas **22**, 103111 (2015).
[17] C. T. Zhou, L. Y. Chew, and X. T. He, Appl. Phys. Lett. **97**, 051502 (2011).
[18] L. L. Ji, J. Snyder, A. Pukhov, R. R. Freeman, and K. U. Akli, arXiv:1509.07018.
[19] T. Nakamura, K. Mima, H. Sakagami, and T. Johzki, Phys. Plasmas **14**, 053112 (2007).
[20] J. Yu, W. Zhou, L. Cao, Z. Zhao, L. Cao, L. Shan, D. Liu, X. Jin, B. Li, and Y. Gu, Appl. Phys. Lett. **100**, 204101 (2012).
[21] L. X. Hu, T. P. Yu, F. Q. Shao, D. B. Zou, and Y. Yin, Phys. Plasmas **22**, 033104 (2015).
[22] J. Snyder, L. L. Ji, and K. U. Akli, arXiv:1603.05596.
[23] S. C. Wilks, W. L. Kruer, M. Tabak, and A. B. Langdon, Phys. Rev. Lett. **69**, 1383 (1992).
[24] A. Pukhov, Z. M. Sheng, and J. Meyer-ter-Vehn, Phys. Plasmas **6**, 2847 (1999).
[25] A. P. L. Robinson, A. V. Arefiev, and D. Neely, Phys. Rev. Lett. **111**, 065002 (2013).
[26] B. Qiao, X. T. He, S. P. Zhu, and C. Y. Zheng, Phys. Plasmas **12**, 083102 (2005).
[27] J. B. Driscoll, X. Liu, S. Yasseri, I. Hsieh, J. I. Dadap, and R. M. Osgood, Opt. Express **17**, 2797 (2009).
[28] B. Cros, C. Courtois, G. Matthieussent, A. Di Bernardo, D. Batani, N. Andreev, and S. Kuznetsov, Phys. Rev. E **65**, 026405 (2002).
[29] J. R. Davies and J. T. Mendonca, Phys. Rev. E **66**, 046604 (2002).
[30] Y. Sentoku and A. J. Kemp, J. Comput. Phys. **227**, 6846 (2008).
[31] J. S. Green, V. M. Ovchinnikov, R. G. Evans, K. U. Akli, H. Azechi, F. N. Beg, C. Bellei, R. R. Freeman, H. Habara, R. Heathcote, M. H. Key, J. A. King, K. L. Lancaster, N. C. Lopes, T. Ma, A. J. MacKinnon, K. Markey, A. McPhee, Z. Najmudin, P. Nilson *et al.*, Phys. Rev. Lett. **100**, 015003 (2008).